Kinetic Tuning of the EF-Hand Calcium Binding Motif: The Gateway Residue Independently Adjusts (i) Barrier Height and (ii) Equilibrium†

Steven K. Drake and Joseph J. Falke*

Department of Chemistry and Biochemistry, University of Colorado, Boulder, Colorado 80309-0215

Received September 29, 1995; Revised Manuscript Received November 27, 1995⊗

ABSTRACT: In EF-hand calcium binding sites of known structure, the side chain provided by the ninth EF-loop position lies at the entrance of the shortest pathway connecting the metal binding cavity to solvent. The location of this residue suggests that it could serve as a "gateway", providing steric and electrostatic control over the kinetics of Ca^{2+} binding and dissociation. To test this hypothesis, the present study has engineered the putative gateway side chain of a model EF-hand site and determined the resulting effects on metal ion affinity and dissociation kinetics. The model site chosen was that of the *Escherichia coli* galactose binding protein (GBP), in which the putative gateway is a Gln side chain. Nine engineered GBP molecules were generated and isolated, each exhibiting native-like activity and global conformation. Two control substitutions at the fourth EF-loop position, a noncoordinating surface residue, had no significant effect on either the equilibrium or the kinetics of the model site. The remaining seven proteins, which possessed unique substitutions at the ninth EF-loop position (Glu, Asn, Asp, Thr, Ser, Gly, Ala), in each case significantly altered the affinity or dissociation kinetics of the site for Tb^{3+}, used as a probe metal ion. Neutral side chains at the gateway position yielded a 590-fold range of Tb^{3+} dissociation kinetics but only a 3-fold range of Tb^{3+} affinities, indicating that the size or polarity of these substitutions alters the transition state barrier for metal binding and release without substantially shifting the equilibrium. In contrast, acidic side chains yielded as much as a 34-fold decrease in the Tb^{3+} off-rate and a 33-fold increase in Tb^{3+} affinity, suggesting that a negative charge at the gateway position increases the equilibrium stability of the bound metal ion and thereby slows metal release. Thus, kinetic tuning by the gateway side chain exhibits both transition state and ground state tuning mechanisms. In natural EF-hand sequences, different gateway side chains are used by slow buffering sites and rapid signaling sites, providing evidence that the gateway position is an important physiological determinant of metal binding kinetics.

The EF-hand calcium binding motif is widely used to activate eukaryotic calcium signaling pathways [reviewed by Bachs et al. (1992), Berridge (1993, 1995), Clapham (1995), Ghosh and Greenberg (1995), Gnegy (1993), Guerini et al. (1990), Putney (1993), and Tsien and Tsien (1990)], and has also been observed in prokaryotic organisms (Swan et al., 1989; Vyas et al., 1987). The heart of this motif, recognized in over 1000 homologous sequences, consists of 2 conserved elements: (i) a 9-residue loop of the γ-turn family, which provides the first 5 metal-coordinating residues, and (ii) a sixth coordinating residue located outside the loop, usually 12 positions from the loop N-terminus, or, equivalently, 3 positions from the loop C-terminus [Kretsinger & Nockolds, 1973; reviewed by Falke et al. (1994), Kawasaki and Kretsinger (1995), Linse and Forsén (1995), Skelton et al. (1994), Marsden et al. (1990), and Strynadka and James (1989)]. Although certain features of the EF-hand motif are universally observed, other aspects are variable. Significantly, the most variable of the coordinating side chain positions is the ninth position of the EF-loop, where the axial side chain appears to block the shortest pathway for Ca^{2+} dissociation from the site, as illustrated in Figure 1. Previous studies have proposed that this side chain acts as a "gateway", serving to tune the kinetics of ion binding and release (Renner et al., 1993). In such a picture, the observed sequence variability at the ninth EF-loop position arises from kinetic tuning, wherein different gateway side chains are utilized by different pathways to optimize the rates of Ca^{2+} binding and release. Both the size and charge of the gateway side chain may be critical for this kinetic tuning (Falke et al., 1994; Renner et al., 1993).

To further test the gateway hypothesis, the present study engineers the gateway position in the Ca^{2+} binding site of the *Escherichia coli* galactose binding protein (GBP). This binding site, which has been structurally characterized by Quicho and co-workers (Vyas et al., 1987), is a useful model EF-hand motif in which to carry out quantitative measurements of kinetic tuning because it exists as a lone, independent, nonallosteric binding site in contrast to the cooperative, multisite binding systems of eukaryotic EF-hands (Falke et al., 1991, 1994; Snyder et al., 1990; Vyas et al., 1989). The GBP molecule also provides a tryptophan indole ring (Trp127) located within 5 Å of the metal binding cavity, facilitating direct optical detection of metal ion binding and release. The phosphorescent Tb^{3+} ion is an ideal probe for such optical measurements, since Tb^{3+} bound in the site can be selectively excited by fluoresence energy transfer from the nearby tryptophan side chain (Snyder et al., 1990). Moreover, Tb^{3+} is similar in size to Ca^{2+} (their effective

† Support provided by NIH Grant GM48203.

* Corresponding author. Telephone: 303-492-3503. Fax: 303-492-5894. Email: falke@colorado.edu.

⊗ Abstract published in *Advance ACS Abstracts,* February 1, 1996.

0006-2960/96/0435-1753$12.00/0

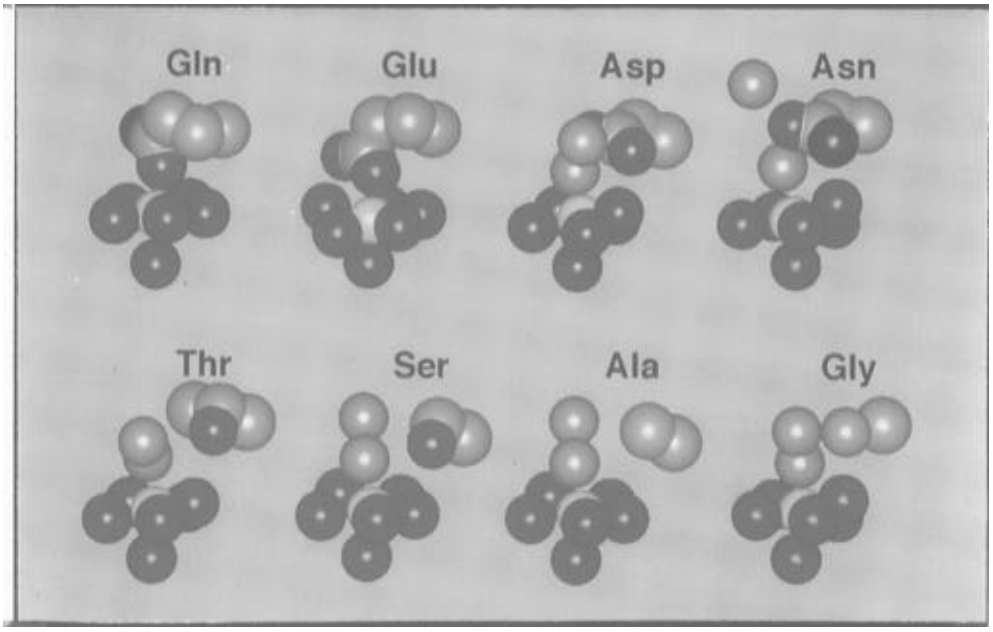

FIGURE 1: Structures illustrating the axial gateway side chain in different EF-hand sites. Shown are representative EF-hand Ca^{2+} coordination motifs from crystallographic or modeled protein structures. Each site possesses seven protein (red) or solvent (aqua) oxygens surrounding the bound Ca^{2+} ion (yellow). All of the sites are identically oriented, with the shortest pathway for Ca^{2+} dissociation leading upward. Highlighted are the gateway side chains bordering the Ca^{2+} dissociation pathway, provided in each case by the ninth EF-loop position. Seven of the structures are from crystallographic coordinates: the native galactose binding protein site (Gln) (Vyas et al., 1987); site I of parvalbumin (Glu) (Kumar et al., 1990); site III of skeletal troponin C (Asp) (Herzberg & James, 1988); site IV of calmodulin (Asn) (Babu et al., 1988); site I of calmodulin (Thr) (Ban et al., Protein Data Bank, Brookhaven); site III of calmodulin (Ser) (Chattopadhyaya et al., 1992); and site II of parvalbumin (Gly) (Kumar et al., 1990). The Ala gateway was modeled by removing the Ser hydroxyl from site III of calmodulin, because such a gateway has not yet been crystallographically described.

ionic radii are 0.98 and 1.06 Å, respectively), and is observed to substitute for Ca^{2+} in functional assays of EF-hand proteins (Horrocks & Albin, 1984; Brittain et al., 1976; Moews & Kretsinger, 1975).

Altogether, 14 substitutions have been incorporated into the model EF-loop, including 12 substitutions at the gateway position. A subset of the resulting engineered GBP molecules is observed to possess stable, well-folded conformations with no detectable structural perturbation outside the Ca^{2+} binding site. The stable substitutions at the gateway position yield striking changes in the Tb^{3+} dissociation kinetics, providing direct evidence that the gateway side chain plays a critical role in kinetic tuning. Moreover, the results reveal two distinct mechanisms of kinetic tuning, one of which adjusts the height of the transition state barrier, while the other alters the stability of the bound metal ion.

METHODS

Protein Engineering and Isolation. The plasmid pSF5 (Falke et al., 1991) containing the GBP gene was subjected to oligonucleotide-directed mutagenesis using standard methods described elsewhere (Falke et al., 1991; Bio-Rad mutagenesis protocol), and the desired point mutations were confirmed by double-stranded DNA sequencing (Tabor & Richardson, 1987; Sanger et al., 1977; US Biochemicals sequencing protocol) or polymerase chain reaction DNA sequencing (Innis et al., 1988; Bio-Rad PCR protocol). These sequencing reactions also examined the regions of the gene outside the targeted mutagenic site, verifying that the engineered plasmids did not contain undesired second-site mutations. Each engineered plasmid was transformed into two *E. coli* strains for protein expression: (i) NM303 (Müller et al., 1985), in which chromosomal expression of GBP has been inactivated, was used to generate protein for metal binding studies; while (ii) W3110 (Drapeau et al., 1968), a tryptophan auxotroph, was utilized to generate GBP labeled with 5-fluorotryptophan for ^{19}F NMR analysis. Expression, purification, and decalcification procedures have been previously described in detail (Falke et al., 1991). The metal-free protein was stored at −70 °C in 100 mM KCl, 10 mM Pipes, pH 6.0 with KOH.

Protein Characterization. The molecular masses of the modified proteins were determined by liquid chromatography directly coupled to a Sciex API-III triple-quadrupole electrospray mass spectrometer (LC/MS), thereby providing an independent check that each molecule contained only the desired point mutation. LC/MS samples were prepared by a 25-fold dilution of protein (100−400 pmol) in storage buffer into 1% formic acid, followed by desalting on a POROS 20R1 capillary HPLC column which injected directly into the mass spectrometer. The protein eluted approximately 10 min after the initiation of a 15 min linear gradient consisting of 1% formic acid with 0−80% acetonitrile.

The activity and structure of each engineered protein were compared to wild type by measuring their affinities for D-galactose, and by obtaining the ^{19}F NMR spectra of the 5-fluorotryptophan-labeled molecules. These ligand binding and NMR measurements were performed as previously described (Falke et al., 1991).

The stabilities of the engineered proteins were compared by measuring their melting temperatures (T_m) as follows. Metal-free protein (2 μM) was equilibrated ~12 h at 25 °C in 100 mM KCl, 10 mM Pipes, pH 6.0 with KOH, and 5 mM $CaCl_2$. A thermal unfolding profile was generated by monitoring the intrinsic tryptophan fluorescence as the

temperature was raised from 30 °C in 2° increments, allowing 15−45 min equilibration at each temperature before measurement. The profile was continued until the sigmoidal melting curve reached a stable base line after the unfolding transition. The resulting data were best fit by nonlinear least squares to a two-state unfolding model as described (Brandts, 1964; Brandts & Hunt, 1967). All fluorescence measurements utilized an SLM48000S spectrofluorometer ($\lambda_{ex} = 285$ nm, $\lambda_{em} = 337$ nm, bandwidths = 4 nm).

Terbium Equilibrium Binding. Two methods were used to measure the Tb^{3+} dissociation constant (K_D). For proteins exhibiting sufficiently low Tb^{3+} affinity ($K_D > 0.5\ \mu$M), the binding of this phosphorescent metal ion was directly monitored by a fluorescence energy transfer assay as previously described (Falke et al., 1991). Briefly, the excitation of intrinsic tryptophans results in energy transfer to the bound Tb^{3+} ion, leading to a steady-state Tb^{3+} phosphorescence which was measured ($\lambda_{ex} = 292$ nm, $\lambda_{em} = 543$ nm, bandwidths = 4 nm). A titration curve was initiated using 2.5 μM metal-free protein equilibrated ~12 h at 25 °C in titration buffer (100 mM KCl, 10 mM Pipes, pH 6.0 with KOH) into which Tb^{3+} was subsequently titrated, allowing 30 min for equilibration after each metal addition prior to measurement. The free Tb^{3+} concentration ($[Tb]_f$) was determined as the difference of the total ($[Tb]_{tot}$) and bound concentrations:

$$[Tb]_f = [Tb]_{tot} - [P]_{tot}\frac{F - F_{min}}{F_{max} - F_{min}} \quad (1)$$

where $[P]_{tot}$ is the total GBP concentration determined by the optical absorbance at 280 nm ($\epsilon_{280} = 42\,850\ M^{-1}\ cm^{-1}$), F is the observed Tb^{3+} emission, F_{min} is the invariant background reading in the absence of Tb^{3+} (less than 4% of F_{max}), and F_{max} is the emission when the site is saturated with Tb^{3+}. The resulting data enabled a Tb^{3+} binding curve to be generated and best fit by nonlinear least-squares analysis using the equation:

$$F = (F_{max} - F_{min})\frac{[Tb]_f}{[Tb]_f + K_D} + F_{min} \quad (2)$$

where K_D is the desired dissociation constant for Tb^{3+} binding to the protein.

Alternatively, for the two engineered proteins exhibiting higher Tb^{3+} affinities (Q142E and Q142D, for which $K_D < 0.5\ \mu$M), a different approach proved more reliable. A competitive binding system was employed in which Tb^{3+} distributed itself between the protein binding site and Indo-1, a fluorescent metal chelator (Linse et al., 1987; Bryant, 1985; Grynkiewicz et al., 1985; Molecular Probes). The ratio of Tb^{3+} bound to the protein and chelator sites, $[Tb_P]_b/[Tb_C]_b$, was measured at 25 °C in titration buffer containing 5 μM chelator and 8 μM protein, to which a subsaturating Tb^{3+} concentration was added and equilibrated for 2 h. The concentration of Tb^{3+} bound to the protein was determined from its phosphorescence ($\lambda_{ex} = 292$ nm; $\lambda_{em} = 543$ nm; bandwidths = 4 nm):

$$[Tb_P]_b = [P]_{tot}\frac{F_{543} - F_{543min}}{F_{543max} - F_{543min}} \quad (3)$$

where the background fluorescence, F_{543min}, varied during the titration due to overlapping fluorescence from apo-Indo-1, necessitating the appropriate correction. Analogously, Tb^{3+} bound to the chelator was quantitated by monitoring the fluorescence of the resulting complex ($\lambda_{ex} = 292$ nm; $\lambda_{em} = 390$ nm; bandwidths = 4 nm):

$$[Tb_C]_b = [C]_{tot}\frac{F_{390} - F_{390min}}{F_{390max} - F_{390min}} \quad (4)$$

where, in this case, F_{390min} was a constant background correction. Finally, the desired K_D of the protein was calculated from the ratio:

$$K_D = K_{DI}\frac{[Tb_C]_b[P]_{tot}}{[Tb_P]_b[C]_{tot}} = K_{DI}\frac{(F_{390} - F_{390min})/(F_{390max} - F_{390min})}{(F_{543} - F_{543min})/(F_{543max} - F_{543min})} \quad (5)$$

where the Tb^{3+} dissociation constant of the chelator, $K_{DI} = 80 \pm 40$ nM, was directly measured by fluorescence titration (25 °C in titration buffer with $\lambda_{ex} = 292$ nm; $\lambda_{em} = 390$ nm; bandwidths = 4 nm). The resulting K_D values for the Q142E and Q142D engineered proteins were found to be significantly higher than previous estimates (Falke et al., 1991), presumably because the high-affinity binding of these mutants precludes accurate estimation of the free metal concentration via eq 1.

Terbium Dissociation Rates. For each of the engineered molecules, the time course of Tb^{3+} dissociation was measured as follows. Metal-free protein (2.5 μM) was equilibrated overnight at 25 °C in titration buffer containing 25 μM $TbCl_3$. Following equilibration, the phosphorescence emission of the bound Tb^{3+} was monitored (see above), and the Tb^{3+} dissociation reaction was triggered by addition of EDTA to 300 μM final concentration, either by syringe injection into a stirred cuvette for the slower dissociating proteins (WT, Q142E, Q142D, K137R, K137G) or by stopped-flow mixing for the rapid sites (Q142A, Q142G, Q142N, Q142S, Q142T; SLM 48000S stopped-flow module). Protein was diluted 2-fold during the stopped flow mixing, yielding a final concentration of 1.2 μM GBP in the rapid site measurements. All time courses were best fit by nonlinear least squares using the equation:

$$F(t)/F(0) = 1 - F_{min}\{1 - \exp(-k_{off}\,t)\} \quad (6)$$

where F_{min} is the background reading and k_{off} is the rate constant for Tb^{3+} dissociation.

Molecular Graphics. Images of EF-hand binding motifs were generated by Insight II graphics software (Version 2.3.5; Biosym) running on a Silicon Graphics Personal Iris 4D/35. Structural coordinates were obtained from the Protein Data Bank (Brookhaven).

RESULTS

Strategy. The gateway hypothesis, which seeks to explain the kinetic tuning of EF-hand Ca^{2+} signaling pathways in molecular terms, proposes that the side chain at the ninth position of the EF-loop is an important determinant of metal binding and dissociation rates (Falke et al., 1994; Renner et al., 1993). Naturally-occurring EF-loops display eight different side chains at this putative gateway position, as

Table 1: Coordinating Residues of EF-Loop Primary Structures[a]

position relative to the N-terminus of the EF-loop					
1 side chain	3 side chain	5 side chain	7 backbone	9 side chain	12[b] side chain
Consensus					
Asp(100%)	Asp(76%)	Asp(52%)	Thr(23%)	Asp(32%)	Glu(92%)
All Sites					
Asp(568)	Asp(432)	Asp(296)	Thr(130)	Asp(181)	Glu(524)
	Asn(131)	Ser(131)	Phe(90)	Ser(116)	Asp(44)
	Ser(5)	Asn(123)	Lys(70)	Thr(79)	
		Thr(9)	Gln(55)	Glu(65)	
		Gly(8)	Tyr(51)	Asn(57)	
		Glu(1)	Glu(36)	Gly(56)	
			Arg(27)	Gln(10)	
			Ser(26)	Cys(4)	
			Ile(15)		
			Cys(13)		
			Asp(11)		
			Leu(11)		
			Val(11)		
			Ala(8)		
			His(6)		
			Met(5)		
			Asn(3)		
Parvalbumin Site 1					
Asp(30)	Asp(30)	Ser(29)	Phe(25)	Glu(30)	Glu(30)
		Glu(1)	Tyr(5)		
Calmodulin Sites 1−4					
Asp(182)	Asp(175)	Asp(99)	Thr(69)	Asp(48)	Glu(181)
	Asn(7)	Asn(79)	Gln(38)	Thr(47)	Asp(1)
		Ser(4)	Phe(26)	Ser(46)	
			Tyr(15)	Asn(40)	
			Cys(13)	Glu(1)[c]	
			Leu(4)		
			His(3)		
			Lys(3)		
			Ser(3)		
			Arg(2)		
			Asn(2)		
			Glu(2)		
			Ala(1)		
			Val(1)		
Troponin C Sites 1−4					
Asp(46)	Asn(25)	Asp(25)	Thr(13)	Asp(38)	Glu(46)
	Asp(21)	Ser(13)	Arg(10)	Ser(8)	
		Gly(8)	Tyr(10)		
			Asp(8)		
			Phe(3)		
			Lys(2)		

[a] EF-hand primary structures were defined by a published search pattern (Falke et al., 1994) applied to the database of Nakayama and Kretsinger (1993). [b] In most, but not all sites, the penultimate coordinating position lies three residues from the C-terminua of the EF-loop, as indicated. [c] Found in the variant calmodulin of *S. cerevisiae*, in which Ca^{2+} binding is not required for its essential function (Davis et al., 1986; Geiser et al., 1991).

illustrated in Table 1: Asp is most common (found in 32% of sequences), followed by Ser (20%), Thr (14%), Glu (11%), Asn (10%), Gly (10%), Gln (2%), and Cys (<1%) (Falke et al., 1994; Kawasaki & Kretsinger, 1995; Marsden et al., 1990; Nakayama & Kretsinger, 1994). To probe the effect of these and other side chains on metal binding to an EF-hand, we constructed a set of engineered GBP molecules in which single substitutions were targeted to either the ninth EF-loop position or a control position within the loop. Subsequently, the engineered proteins were checked for global perturbations by analysis of their thermal stability, galactose affinity, and conformation. Finally, the metal binding affinity and dissociation rate of each engineered site were quantitated, thereby defining the range of equilibrium and kinetic tuning afforded by different side chains at the ninth EF-loop position.

Table 2: EF-Loop Side Chain Substitutions

site	gateway side chain[a]	volume[b] (Å^2)
Q142R	Arg	100
Q142M	Met	76
Q142L	Leu	76
WT(Q142)	Gln[d,e]	66
(K137R)[c]	Gln[d,e]	66
(K137G)[c]	Gln[d,e]	66
Q142E	Glu[d,e]	61
Q142V	Val	57
Q142N	Asn[d,e]	48
Q142T	Thr[d,e]	45
Q142D	Asp[d,e]	43
Q142C	Cys[d]	38
Q142S	Ser[d,e]	25
Q142A	Ala[e]	19
Q142G	Gly[d,e]	0

[a] In order of decreasing volume. [b] Determined by subtracting Gly from the free amino acid. [c] Control substitution at surface-exposed position 4 of the EF-loop. [d] Observed in natural EF-hand sequences (see Table 1). [e] Successfully overexpressed and isolated in this study.

The metal ion probe chosen for the present measurements was Tb^{3+}, which can be monitored by a sensitive fluorescence energy transfer assay, and which substitutes well for Ca^{2+} in EF-hand systems [for examples, see Burroughs et al. (1994), Snyder et al. (1990), Horrocks and Albin (1984), Brittain et al. (1976), and Moews and Kretsinger (1975)]. It was not possible to measure Ca^{2+} dissociation kinetics directly, since (i) Ca^{2+} binding to GBP cannot be monitored optically, and (ii) high concentrations (≥ 50 μM) of the fluorescent Ca^{2+} chelators successfully used to measure Ca^{2+} dissociation kinetics in other systems (Martin et al., 1985) have been shown to perturb GBP (Renner et al., 1993).

Construction and Isolation of Engineered Proteins. Engineered proteins were generated by oligonucleotide-directed mutagenesis of the GBP gene. Altogether 15 different GBP molecules were investigated, including the wild-type protein (WT), as summarized in Table 2. Eight of these proteins possessed a naturally-occurring side chain at the ninth EF-loop position [Gln(WT), Glu, Asn, Asp, Thr, Ser, Gly, Cys], while five possessed a side chain not yet observed at this location (Arg, Met, Leu, Val, Ala). Together these 13 side chains provided a range of side chain volume, shape, hydrophobicity, polarity, charge, and hydrogen-bonding potential. The remaining two engineered proteins, serving as negative controls, each possessed a single substitution at the noncoordinating fourth position of the EF-loop, where a surface-exposed Lys residue was altered by either a conservative or a nonconservative replacement (Arg or Gly, respectively).

Interestingly, five of the engineered proteins were poorly expressed by *E. coli*, suggesting that certain substitutions can inhibit the synthesis of GBP or destabilize the folded protein *in vivo*. The side chain observed with the lowest frequency in natural sequences (Cys, <1%) as well as four side chains never observed at the ninth EF-loop position (Arg, Met, Leu, Val) each yielded undetectable levels of expression (<5% of overexpressed WT). The remaining 10 native and engineered GBP molecules were expressed to relatively high levels (≥25% WT), enabling their purification to ≥90% homogeneity by standard methods. The identity

Table 3: Effects of EF-Loop Substitutions on Stability, Ligand Binding, and Conformation

site	gateway side chain[a]	protein molecular mass: predicted (Da)	protein molecular mass: measured[b] (±4 Da)	T_m[c] (°C)	K_D(Gal)[d] (μM)	^{19}F NMR chemical shift[e] (±0.1 ppm): W284	W195	W183	W133	W127
WT(Q142)	Gln	33368	33370	58.5	0.5 ± 0.1	52.5	48.4	42.9	51.2, 51.9	46.0, 46.2
(K137R)	Gln	33398	33399	58.6	0.7 ± 0.3	52.5	48.3	42.8	51.2, 51.8	46.0, 46.2
(K137G)	Gln	33299	33298	58.1	0.6 ± 0.2	52.5	48.3	42.8	51.2, 51.8	46.0, 46.2
Q142E[f]	Glu	33369	33368	53.4	0.3 ± 0.1	52.4	48.3	42.8	51.0, 51.5	46.1, 46.2
Q142N[f]	Asn	33354	33353	54.4	0.5 ± 0.1	52.5	48.3	42.7	51.4, 52.0	45.7, 45.8
Q142T	Thr	33341	33337	52.7	0.3 ± 0.1	52.5	48.5	42.8	50.8, 51.5	46.3, 46.5
Q142D[f]	Asp	33355	33354	52.6	0.6 ± 0.1	52.5	48.3	42.7	51.3, 52.0	46.3, 46.5
Q142S	Ser	33327	33324	54.0	0.4 ± 0.3	52.5	48.3	42.8	50.8, 51.5	46.6, 46.9
Q142A	Ala	33311	33310	53.7	0.9 ± 0.4	52.5	48.2	42.7	51.0, 51.6	46.6, 46.8
Q142G	Gly	33297	33296	53.6	0.2 ± 0.1	52.5	48.3	42.8	51.2, 51.8	46.4, 46.5

[a] In order of decreasing volume. [b] Molecular mass of apoprotein measured by electrospray mass spectrometry. [c] Melting temperature in the presence of Ca. [d] Equilibrium dissociation constant for D-galactose. [e] ^{19}F NMR chemical shifts of 5-fluorotryptophan resonances. [f] D-Galactose binding data and ^{19}F NMR chemical shifts from Falke et al. (1991).

of each purified protein was checked by electrospray mass spectrometry, which confirmed the expected molecular masses as summarized in Table 3.

Characterization of Engineered Proteins. The nine well-expressed mutants were tested for global perturbations by comparing their thermal stabilities, galactose affinities, and ^{19}F-NMR spectra to those of the native protein, as summarized in Table 3. All seven substitutions at the gateway position reduced the thermal stability observed in the presence of saturating Ca^{2+} ion by approximately 5 °C relative to the wild-type Gln ($T_m = 53 \pm 1$ °C for Glu, Asp, Asn, Thr, Ser, Ala, and Gly; while $T_m = 58.5$ °C for Gln). The destabilizing effect of these substitutions verifies both the role of the GBP Ca^{2+} binding site in maintaining the folded protein structure (Vyas et al., 1987) and the importance of the gateway position to this stabilization. By contrast, the two negative control substitutions at the fourth position had little or no effect on thermal stability (Table 3). Overall, all nine of the isolated mutants were stable and well-folded proteins, exhibiting equally sharp melting transitions (data not shown).

EF-Loop substitutions had little effect on the affinity of the protein for D-galactose, which occupies a cleft 27 Å from the Ca^{2+} binding site. Of the nine engineered EF-loops, eight yielded D-galactose dissociation constants (K_D) which were within error of the native protein (Table 3). The one exception was the Gly substitution at the ninth EF-loop position, which increased the sugar affinity 2.5-fold.

EF-Loop substitutions did not significantly alter the ^{19}F NMR chemical shifts of probe residues located outside the Ca^{2+} binding site. Table 3 summarizes the ^{19}F NMR spectra obtained for engineered GBP labeled with 5-fluorotryptophan at each of its five tryptophan positions. The three distant probes, Trp195, Trp183, and Trp284, which lie 16, 26, and 41 Å from the bound metal ion, respectively, exhibited no detectable significant chemical shift changes upon EF-loop substitution. The other two probe positions, Trp133 and Trp127, are located near Asp134, the N-terminus of the loop. The indole ring of Trp127 lies within 5 Å of the bound metal, and also directly contacts the indole of Trp 133. Each substitution at the ninth loop position triggered detectable chemical shift changes for one or both of these internal probes, while the control substitutions were nonperturbing. Since ^{19}F chemical shifts have been shown to be exquisitely sensitive to local structure and electrostatics in this and other proteins [reviewed by Danielson and Falke (1995, 1996)], the ^{19}F NMR data of Table 3 indicate that substitutions at the ninth position cause structural changes that are localized to the Ca^{2+} binding region, as designed. In summary, the observed effects of engineered EF-loops confirm the role of the native Ca^{2+} binding site in maximizing the thermal stability of GBP, while the sugar affinities and overall conformations of the engineered proteins indicate that the tested substitutions do not cause significant long-range perturbations.

Table 4: Effects of EF-Loop Substitutions on Tb^{3+} Affinity and Off-Rate

site[a]	gateway side chain	$K_D(Tb^{3+})$[b] (μM)	$k_{off}(Tb^{3+})$[c] (s^{-1})
Q142E	Glu	0.06 ± 0.03	$(1.86 \pm 0.02) \times 10^{-4}$
Q142D	Asp	0.13 ± 0.08	$(1.87 \pm 0.01) \times 10^{-3}$
(K137G)	Gln	1.8 ± 0.2	$(6.34 \pm 0.03) \times 10^{-3}$
WT(Q142)	Gln	2.0 ± 0.5	$(6.41 \pm 0.03) \times 10^{-3}$
(K137R)	Gln	3.0 ± 0.6	$(7.90 \pm 0.05) \times 10^{-3}$
Q142S	Ser	0.8 ± 0.1	$(6.5 \pm 0.1) \times 10^{-1}$
Q142T	Thr	2.3 ± 0.2	$(9.1 \pm 0.3) \times 10^{-1}$
Q142N	Asn	1.9 ± 0.3	$(1.02 \pm 0.03) \times 10^{0}$
Q142G	Gly	1.4 ± 0.4	$(2.00 \pm 0.05) \times 10^{0}$
Q142A	Ala	2.8 ± 0.2	$(3.79 \pm 0.08) \times 10^{0}$

[a] Listed in order of increasing $k_{off}(Tb^{3+})$. [b] Equilibrium dissociation constant for Tb^{3+} at 25 °C. [c] Rate constant for Tb^{3+} dissociation at 25 °C.

Effect of EF-Loop Substitutions on Metal Binding Affinity. Using direct Tb^{3+} binding measurements developed for this study (see Methods), the Tb^{3+} affinities of the nine engineered proteins were measured and compared to that of native GBP. Table 4 presents the resulting Tb^{3+} dissociation constants (K_D), which form a striking pattern. Proteins possessing a neutral side chain at the ninth EF-loop position [Gln(WT), Asn, Thr, Ser, Ala, Gly] yield K_D values spanning less than a 3-fold range; similarly, the two negative control substitutions have no significant effect on Tb^{3+} affinity. In contrast, the two molecules possessing an acidic side chain at the ninth loop position exhibit considerably higher affinities for Tb^{3+}: fully 33-fold higher affinity for the Glu side chain, and 15-fold higher for Asp relative to the wild-type affinity. (It should be noted that the previously published affinities of the Q142E and Q142D mutants were serious underestimates, as discussed under Methods.) Thus, the Tb^{3+} affinity of the EF-loop appears to be highly sensitive to the charge of the gateway position, but is relatively insensitive to other structural and electrostatic features of the gateway side chain.

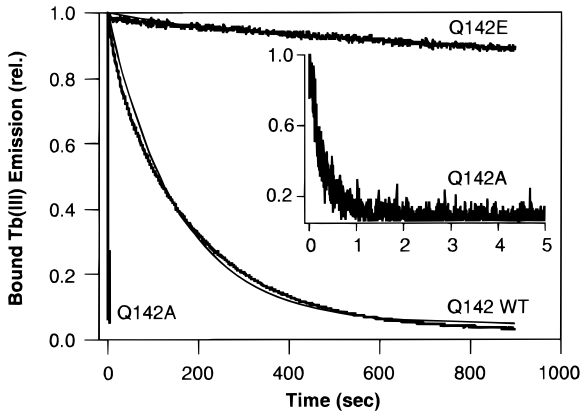

FIGURE 2: Tb^{3+} dissociation time courses of the native and engineered EF-hand model site. Shown are representative results, including the fastest (Q142A) and slowest (Q142E) Tb^{3+} dissociation reactions. Each time course plots the optical emission of bound Tb^{3+} ion in the EF-hand site of a wild type or engineered galactose binding protein. The dissociation reaction, which was triggered by the addition of excess EDTA at zero time, was monitored as the subsequent decrease in the bound Tb^{3+} emission, yielding a dissociation time course that was fit by nonlinear least-squares analysis (smooth curves). Dissociation reactions at 25 °C consisted of 2.5 μM protein, 25 μM $TbCl_3$, 100 mM KCl, 10 mM Pipes, pH to 6.0 with KOH, and 300 μM EDTA. Rapid reactions, such as that of the Q142A mutant (inset), were measured by stopped-flow.

Effect of EF-Loop Substitutions on Metal Dissociation Kinetics. Figure 2 and Table 4 compare the Tb^{3+} dissociation rates of the engineered and native GBP molecules. The dissociation rates observed for substitutions at the ninth EF-loop position span over 4 orders of magnitude: the slowest rates are associated with the acidic substitutions at the gateway position (2×10^{-3} or 2×10^{-4} s^{-1} $molecule^{-1}$ for Asp or Glu, respectively), while the fastest rates are provided by small, nonpolar side chains (2 or 4 s^{-1} $molecule^{-1}$ for Gly or Ala, respectively). The corresponding lifetimes of Tb^{3+} in the site range from 5000 s to 0.2 s. The two negative control substitutions at the fourth EF-loop position, by contrast, have no significant effect on metal dissociation kinetics. Together these results indicate that the kinetics of metal dissociation are highly dependent on the nature of the gateway side chain at the ninth EF-loop position.

DISCUSSION

The observed equilibrium and kinetic effects of side chain substitutions directly establish the importance of the ninth EF-loop position, termed the "gateway" position, in tuning the kinetic properties of the EF-hand Ca^{2+} binding motif. Overall, the results suggest that both the size and electrostatic features of the gateway side chain play critical roles in kinetic tuning. The gateway regions characterized by the present study are summarized in Figure 1, which displays the crystallographic or modeled structure of each region, including the position of the gateway side chain.

The gateway side chain is observed to tune the kinetics of metal binding and dissociation by two distinct mechanisms, as illustrated in Figure 3. The first, termed ground state tuning, adjusts the energetics of the bound ion within the site, thereby selectively controlling the rate of ion release. For example, when the native Gln side chain of the model site is substituted with an acidic Glu or Asp side chain, the observed affinity for the Tb^{3+} ion increases substantially. The largest effect is seen for the longer Glu side chain, which

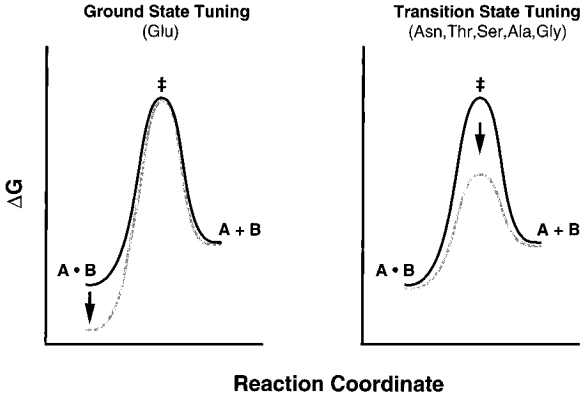

FIGURE 3: Two mechanisms for tuning the kinetics of binding and release. Shown is a thermodynamic reaction pathway for metal binding and dissociation at an EF-hand site. The kinetics of ion dissociation can be tuned by altering either (i) the stability of the bound ion, thereby shifting the binding equilibrium, or (ii) the barrier height of the rate-limiting step, thereby changing the on- and off-rates by identical factors.

provides direct metal coordination in all eight known structures of EF-hands containing this residue [reviewed by Falke et al. (1994)]. In the GBP site, substitution of Glu into the gateway position increases the Tb^{3+} affinity 33-fold, while decreasing the Tb^{3+} dissociation rate 34-fold, or by nearly the same factor (Table 4). By contrast, the calculated Tb^{3+} association rate remains virtually unchanged ($k_{on} = k_{off}/K_D$). The simplest interpretation of these results is that the Glu gateway side chain selectively stabilizes the occupied site, thereby providing pure ground state tuning of the complex formed between the metal ion and the protein (Figure 3). The magnitude of this stabilization, on the order of 2 kcal mol^{-1}, also appears in a comparison of the previously determined Arrhenius activation energies for the Glu mutant ($E_A = 12$ kcal mol^{-1}) and the native site ($E_A =$ 10 kcal mol^{-1}; Renner et al., 1993).

The second type of kinetic tuning, termed transition state tuning, adjusts the height of the transition state barrier (Figure 3). The altered barrier height, in turn, modifies the association and dissociation rates by the same factor without changing the binding equilibrium (Falke et al., 1994; Renner et al., 1993). For example, the present study compares six neutral gateway side chains, Gln, Asn, Thr, Ser, Ala, and Gly, which are observed to provide Tb^{3+} dissociation kinetics spanning a 590-fold range, while their Tb^{3+} affinities vary less than 3-fold (Table 4). Such findings clearly demonstrate that uncharged gateway residues are able to selectively adjust only the barrier height of the reaction pathway, without perturbing the equilibrium between the occupied and unoccupied sites (Figure 3). It follows that neutral gateway substitutions tune the kinetics of metal ion binding and release independently of the binding affinity, so that, in principle, an EF-hand site in a given signaling pathway could be simultaneously optimized for both its (i) Ca^{2+} affinity and (ii) speed of activation or inactivation.

Transition state tuning appears to stem from the size and polarity of the gateway side chain. Comparing the six neutral side chains, the slowest dissociation is observed for the longest residue, Gln, which is known to provide direct coordination of bound metal ion in the model site (Table 4, Figure 1). Shorter side chains, by contrast, have never been observed to directly coordinate metal in any of the 38 examples described in protein crystal structures (Falke et al.,

1994); instead, the latter sites always utilize a coordinating water molecule at the gateway location (Figure 1). When substituted into the GBP site, each of these shorter gateway side chains provide faster Tb^{3+} association and dissociation kinetics than the directly coordinating Gln residue, suggesting that axial water coordination imposes a smaller barrier to metal binding and release than a side chain. The resulting barrier height lowering has been directly observed for one gateway substitution, Asn, by measurement of the Arrhenius activation energy (Renner et al., 1993). The fastest Tb^{3+} kinetics are observed for the smallest side chains, Ala and Gly. In addition to their small size, which minimizes steric constraints on the reaction pathway, these side chains lack the hydrogen-bonding capacity possessed by the other gateway residues tested; thus, they are unable to order the surrounding solvent through the formation of hydrogen bonds. The present data do not resolve whether the effect of these side chains on the reaction kinetics is dominated by their small size or low polarity.

Finally, substitution of Asp for Gln at the ninth EF-loop position appears to tune both the ground and transition states. This substitution generates a 15-fold increase in Tb^{3+} affinity while the Tb^{3+} dissociation rate is decreased only 3-fold (Table 4), indicating a 5-fold increase in the calculated Tb^{3+} association rate. The simplest molecular explanation for this combination of equilibrium and kinetic effects is that the substitution simultaneously increases the stability of the bound ion, and lowers the transition state barrier. The effect of the negatively charged Asp carboxylate on the binding equilibrium is smaller than that of Glu, since the Asp side chain does not directly coordinate the bound ion as does the longer Glu side chain (Figure 1) (Falke et al., 1994). Overall, this example emphasizes that the affinity and kinetics of the EF-hand motif are tuned by both the charge and structure of the gateway side chain.

The biological importance of gateway tuning is illustrated by a comparison of EF-hand sites from proteins with different functions. Table 1 contrasts the primary structures of sites from the parvalbumin family with those of the calmodulin and troponin C families. The parvalbumins, which provide buffering in muscle contraction pathways, are characterized by their slow divalent metal dissociation rates and their extremely high Ca^{2+} affinities, which are both critical for normal function of the contraction signal [Hou et al., 1992; Pechére et al., 1977; reviewed by Falke et al. (1994) and Ashley et al. (1991)]. All of the existing parvalbumin primary structures (30 examples) possess Glu at the gateway position of their first EF-loop, consistent with the proposal that this side chain provides the greatest thermodynamic stabilization of bound metal, and the maximum kinetic barrier to metal release. In contrast, the EF-hand sites of the calmodulin−troponin C family possess significantly faster Ca^{2+} dissociation kinetics and lower affinities matched to cytoplasmic Ca^{2+} levels, as predicated by their role as rapid "on−off switches" in Ca^{2+} signaling pathways. The gateway positions of these sites (228 examples) never utilize Glu or even Gln; instead, the shorter side chains observed provide the rapid ion binding and release required for Ca^{2+} signaling [Martin et al., 1985; Potter & Johnson, 1982; reviewed by Falke et al. (1994) and Ashley et al. (1991)]. The only exception is site II of the variant calmodulin from the yeast *Saccharomyces cerevisiae*, which utilizes Glu as the gateway side chain (Starovasnik et al., 1993; Davis et al., 1986). However, unlike the other members of the calmodulin−troponin C superfamily, the EF-hand Ca^{2+} binding sites of this protein are not required for its essential function (Geiser et al., 1991), indicating that it may have evolved a non-Ca^{2+} signaling role. Thus, a perfect correlation is observed between the identity of the gateway side chain and EF-hand function. Although EF-hand kinetics can be further modulated by other features of the EF-loop (Drake and Falke, in preparation) or by interprotein interactions (Peersen and Falke, submitted for publication), the available evidence suggests that the gateway position plays a critical role in tuning the activation parameters of Ca^{2+} signaling pathways.

Finally, the effects of EF-loop substitutions on GBP stability confirm the structural role proposed for the model site, which stabilizes the folded protein in the proteolytic environment of the periplasm (Vyas et al., 1987). All substitutions examined at the gateway position either (i) dramatically reduce protein expression in *E. coli* or (ii) slightly decrease the thermal stability of GBP. Interestingly, of the five side chains tested which are not utilized in naturally-occurring EF-loops, four block GBP expression (Arg, Met, Leu, Val), as does the side chain observed least frequently in natural sites (Cys; Table 1). Thus, it is likely that biological systems avoid such side chains because they block Ca^{2+} binding, or otherwise destabilize the EF-hand motif. Although most EF-hand sites are thought to play roles in Ca^{2+} signaling pathways, it remains to be determined what fraction of the known EF-loops is utilized for protein stabilization.

ACKNOWLEDGMENT

We thank Drs. Andrea Hazard, Olve Peersen, and Katheryn Resing for helpful discussions, Theodore Chen and Keith Lee for expert technical assistance, and NIH Grant GM48203 for funding.

REFERENCES

Ashley, C. C., Mulligan, I. P., & Lea, T. J. (1991) *Q. Rev. Biophys. 24*, 1−73.
Babu, Y. S., Bugg, C. E., & Cook, W. J. (1988) *J. Mol. Biol. 204*, 191−204.
Bachs, O., Agell, N., & Carafoli, E. (1992) *Biochim. Biophys. Acta 1113*, 259−270.
Berridge, M. J. (1993) *Nature 361*, 315−325.
Berridge, M. J. (1995) *BioEssays 17*, 491−500.
Brandts, J. F. (1964) *J. Am. Chem. Soc. 86*, 4291−4301.
Brandts, J. F., & Hunt, L. (1967) *J. Am. Chem. Soc. 89*, 4826−4838.
Brittain, H. G., Richardson, F. S., & Martin, R. B. (1976) *J. Am. Chem. Soc. 98*, 8255−8260.
Bryant, D. T. W. (1985) *Biochem. J. 226*, 613−616.
Burroughs, S. E., Horrocks, W. D., Ren, H., & Klee, C. B. (1994) *Biochemistry 33*, 10428−10436.
Chattopadhyaya, R., Meador, W. E., Means, A. R., & Quiocho, F. A. (1992) *J. Mol. Biol. 228*, 1177−1192.
Clapham, D. E. (1995) *Cell 80*, 259−268.
Danielson, M. A., & Falke, J. J. (1995) *Encycl. Nucl. Magn. Reson.* (in press).
Danielson, M. A., & Falke, J. J. (1996) *Annu. Rev. Biophys. Biomol. Struct.* (in press).
Davis, T. N., Urdea, M. S., Masiarz, F. R., & Thorner, J. (1986) *Cell 47*, 423−431.
Drapeau, G. R., Brammar, W. J., & Yanofsky, C. (1968) *J. Mol. Biol. 35*, 357−367.
Falke, J. J., Snyder, E. E., Thatcher, K. C., & Voertler, C. S. (1991) *Biochemistry 30*, 8690−8697.

Falke, J. J., Drake, S. K., Hazard, A. L., & Peersen, O. B. (1994) *Q. Rev. Biophys. 27*, 219−290.
Geiser, J. R., van Tuinen, D., Brockerhoff, S. E., Neff, M. M., & Davis, T. N. (1991) *Cell 65*, 949−959.
Ghosh, A., & Greenberg, M. E. (1995) *Science 268*, 239−247.
Gnegy, M. E. (1993) *Annu. Rev. Pharmicol. Toxicol. 33*, 45−70.
Grynkiewicz, G., Poenie, M., & Tsien, R. Y. (1985) *J. Biol. Chem. 260*, 3440−3450.
Guerini, D., Hubbard, M. J., Krinks, M. H., & Klee, C. B. (1990) *Adv. Second Messenger Phosphoprotein Res. 24*, 242−247.
Herzberg, O., & James, M. N. G. (1988) *J. Mol. Biol. 203*, 761−779.
Horrocks, W. D., & Albin, M. (1984) *Prog. Inorg. Chem. 31*, 1−104.
Hou, T. T., Johnson, J. D., & Rall, J. A. (1992) *J. Physiol. (London) 449*, 399−410.
Innis, M. A., Myambo, K. B., Gelfand, D. H., & Brow, M. A. D. (1988) *Proc. Natl. Acad. Sci. U.S.A. 85*, 9436−9440.
Kawasaki, H., & Kresinger, R. H. (1995) *Protein Profiles 2*, 305−490.
Kretsinger, R. H., & Nockolds, C. E. (1973) *J. Biol. Chem. 248*, 3313−3326.
Kumar, V. D., Lee, L., & Edwards, B. F. P. (1990) *Biochemistry 29*, 1404−1412.
Linse, S., & Forsén, S. (1995) *Adv. Second Messenger Phosphoprotein Res. 30*, 89−151.
Linse, S., Brodin, P., Drakenberg, T., Thulin, E., Sellers, P., Elmdén, K., Grundström, T., & Forsén, S. (1987) *Biochemistry 26*, 6723−6735.
Marsden, B. J., Shaw, G. S., & Sykes, B. D. (1990) *Biochem. Cell Biol. 68*, 587−601.
Martin, S. R., Andersson Teleman, A., Bayley, P. M., Drakenberg, T., & Forsén, S. (1985) *Eur. J. Biochem. 151*, 543−550.
Moews, P. C., & Kretsinger, R. H. (1975) *J. Mol. Biol. 91*, 229−232.
Müller, N., Heine, H.-G., & Boos, W. (1985) *J. Bacteriol. 163*, 37−45.
Nakayama, S., & Kretsinger, R. H. (1993) *J. Mol. Evol. 36*, 458−476.
Nakayama, S., & Kretsinger, R. H. (1994) *Annu. Rev. Biophys. Biomol. Struct. 23*, 473−507.
Pechère, J. F., Derancourt, J., & Haiech, J. (1977) *FEBS Lett. 75*, 111−114.
Potter, J. D., & Johnson, J. D. (1982) *Calcium Cell Funct. 2*, 145−173.
Putney, J. W. (1993) *Science 262*, 676−678.
Renner, M., Danielson, M. A., & Falke, J. J. (1993) *Proc. Natl. Acad. Sci. U.S.A. 90*, 6493−6497.
Sanger, F., Nicklen, S., & Coulson, A. R. (1977) *Proc. Natl. Acad. Sci. U.S.A. 74*, 5463−5467.
Skelton, N. J., Kördel, J., Akke, M., Forsén, S., & Chazin, W. J. (1994) *Nat. Struct. Biol. 1*, 239−245.
Snyder, E. E., Buoscio, B. W., & Falke, J. J. (1990) *Biochemistry 29*, 3937−3943.
Starovasnik, M. A., Davis, T. N., & Klevit, R. E. (1993) *Biochemistry 32*, 3261−3270.
Strynadka, N. C. J., & James, M. N. G. (1989) *Annu. Rev. Biochem. 58*, 951−998.
Swan, D. G., Cortes, J., Hale, R. S., & Leadlay, P. F. (1989) *J. Bacteriol. 171*, 5614−5619.
Tabor, S., & Richardson, C. C. (1987) *Proc. Natl. Acad. Sci. U.S.A. 84*, 4767−4771.
Tsien, R. W., & Tsien, R. Y. (1990) *Annu. Rev. Cell Biol. 6*, 715−760.
Vyas, N. K., Vyas, M. N., & Quiocho, F. A. (1987) *Nature 327*, 635−638.
Vyas, M. N., Jacobson, B. L., & Quiocho, F. A. (1989) *J. Biol. Chem. 264*, 20817−20821.

BI952335C